Available online at www.sciencedirect.com
SCIENCE DIRECT®
International Journal of Solids and Structures 42 (2005) 663–680
INTERNATIONAL JOURNAL OF SOLIDS and STRUCTURES
www.elsevier.com/locate/ijsolstr

Development of a methodology for determination of interface fracture toughness of laminate composites—the 0°/90° pair

Leslie Banks-Sills *, Vinodkumar Boniface [1], Rami Eliasi

The Dreszer Fracture Mechanics Laboratory, Department of Solid Mechanics, Materials and Systems, The Fleischman Faculty of Engineering, Tel Aviv University, Ramat Aviv 69978, Israel

Received 18 April 2004; received in revised form 14 June 2004
Available online 21 August 2004

Abstract

Experiments are carried out to determine the delamination toughness for a crack along the interface between two transversely isotropic materials. The material chosen for study consists of carbon fibers embedded within an epoxy matrix. A crack is introduced between two layers of this material, with fibers in the upper layer along the 0°-direction and those in the lower layer along the 90°-direction. The Brazilian disk specimen is employed in the testing. Finite element analyses are carried out to determine stress intensity factors arising from the applied load. Residual stresses resulting from the curing process create transverse cracks in the 90°-layer. Stress intensity factors pertaining to this stress field are obtained, as well. These stress intensity factors are superposed with those from the applied load to obtain the total stress intensity factor. From the load at fracture, the critical interface energy release rate $\mathcal{G}_{ic}$ as a function of phase angle ψ is determined, and results are compared to a fracture criterion. Two lay-ups of the carbon fiber/epoxy material are examined.

Keywords: Delamination; Fracture toughness; Fiber-reinforced composite material; Layered material; Finite elements

* Corresponding author. Tel.: +972 3640 8132; fax: +972 3640 7617.
E-mail addresses: banks@eng.tau.ac.il (L. Banks-Sills), vinodkumar.boniface@geind.ge.com (V. Boniface), eliasi@eng.tau.ac.il (R. Eliasi).
[1] Present address: Engineering Analysis Center of Excellence, GE-India Technology Center, Bangalore 560 066, India.

0020-7683/$ - see front matter
doi:10.1016/j.ijsolstr.2004.06.025

1. Introduction

In recent years, much research has been directed toward understanding interface fracture. Investigators have concentrated on the problem of an interface between two isotropic, homogeneous bodies. Another area of interest is the delamination of two unidirectional composite layers in different directions. In particular, the toughness of a 0°/90° interface in a composite material consisting of carbon fibers embedded in an epoxy matrix is studied here.

Most studies on the fracture toughness of fiber composite materials have focused on unidirectional composites (Jurf and Pipes, 1982; Whitney et al., 1982; Aliyu and Daniel, 1985; Gillespie et al., 1987; Davies et al., 1990; Hashemi et al., 1990; Reeder and Crews, 1990; Yoon and Hong, 1990; Kinloch et al., 1993; Bansal and Kumosa, 1995; Zhao et al., 1995; Liu et al., 1997; Rikards et al., 1998, for example). Liu et al. (1997) employed the Brazilian disk specimen to determine the fracture toughness of uniaxial laminate composites with a crack in the direction of the fibers, as well as perpendicular to them. As noted by the authors, a wide range of mixed modes is obtained with this specimen. Moreover, there are two ASTM standards (D 5528-94a, 2001; D 6671-01, 2002) for measuring interlaminar toughness of unidirectional fiber-reinforced polymer composites. The first, D 5528-94a is used for measuring mode I interlaminar toughness; whereas, D 6671-01 is used for measuring mixed mode (modes I and II) interlaminar toughness.

There have also been studies of interface fracture toughness for a crack between two laminae of different directions (Wilkins et al., 1982; Chai, 1984; Laksimi et al., 1991; Hwu et al., 1995; Polaha et al., 1996; Buchholz et al., 1997; Choi et al., 1999). As early as 1982, Wilkins et al. (1982) applied the fundamentals of fracture mechanics to delamination growth in fiber-reinforced composites.

Hwu et al. (1995) employed four specimens to examine the interface (or delamination) toughness of glass/epoxy laminated specimens mostly with the lay-up $0_4^\circ/\theta_4^+/\theta_4^-/0_4^\circ$. The double cantilever beam (DCB) specimen produced nearly mode I behavior, whereas the edge-notched flexural (ENF) specimen yielded nearly mode II behavior. The interface fracture toughness for each mode was determined by means of the finite element method and a crack closure integral. Two values for the total $\mathscr{G}_c$ were presented, one obtained from the finite element calculations and one from compliance of the specimen. These results showed that for the nearly mode I specimen, the other modes do not contribute much to the total critical energy release rate. A similar observation was made for the ENF specimen. The fracture toughness for nearly pure modes I and II were within the scatter of those obtained for unidirectional composite materials. Two other specimens (cracked-lap shear, CLS, and modified end-notched flexural, MENF) yielded mixed modes each within rather narrow ranges. A fracture criterion was obtained by means of a curve fit.

Delamination toughness tests were carried out by Polaha et al. (1996) on carbon/epoxy composite specimens with 0°/0°, 15°/15°, 15°/−15°, 30°/30° and 30°/−30° interfaces. Three mode ratios were considered: nearly mode I, nearly mode II and mixed mode with $\mathscr{G}_{II}/\mathscr{G}_I \simeq 0.7$. Interpretation of modes was made by neglecting the oscillatory nature of the stress and displacement fields at the crack tip. Hence, the exact modes were not attained. In addition, the effect of residual stresses was neglected. Toughness values were obtained from specimens with both induced natural cracks and thin notches. Much scatter in the data may be noted. For mode I deformation, toughness values decrease as fiber angle increases. For mode II, there is nearly no influence of fiber angle. For mode I, except for the 0°/0° interface, there is only a small difference between the toughness values for cracked and notched specimens. For mode II, the toughness values are generally lower for the cracked specimens. For the one mixed mode ratio examined, there was a weak decrease in the toughness values as ply angle decreased for the notched specimens. As with mode II, the average toughness of the cracked specimens is lower than those containing notches. Although this difference decreases with increasing angle.

Choi et al. (1999) measured the fracture toughness for fiber-reinforced carbon/epoxy material. Most specimens consisted of 24 layers $(-45°/0°/+45°)_{2s}$ $(+45°/0°/-45°)_{2s}$ with the initial delamination on the +45°/−45° mid-plane of the specimen. Complex loading paths were discerned as the crack propagated

through the multi-directional fiber composite. Nonetheless, an initiation interface fracture toughness was measured which was greater for the multi-directional laminates than for the unidirectional (0°/0°) composite. In addition, for nearly mode I deformation, some specimens with a $(+45°/-45°)_{12}$ lay-up were tested. Values of the initiation $\mathscr{G}_{Ic}$ measured by these specimens were lower than for the multi-directional specimens.

There have been many studies using the DCB specimen to measure nearly mode I deformation and the ENF specimen for nearly mode II deformation. See for example, Sun and Zheng (1996), where many of the problems of these specimens are discussed and other references given. Buchholz et al. (1997) compared seven data reduction methods for DCB tests on glass/epoxy composites. It may be observed that the $\mathscr{G}_{Ic}$ values vary with the method applied.

In this investigation, a methodology is developed for measuring the interface fracture toughness or delamination toughness of fiber-reinforced material such as carbon/epoxy (AS4/3502). The specimen configuration chosen for this study is the Brazilian disk, as it allows for a wide range of mode mixities. The Brazilian disk specimens employed here are shown in Fig. 1a and b; they are modified from the bimaterial specimen in Fig. 1c. In Fig. 1a, there is a composite strip consisting of three layers of approximate thickness 4.2 mm each in the 0°/90°/0° directions. It is glued to aluminum partial disks. In Fig. 1b, the inner three layers are approximately 0.54 mm thick with the same directions as those in Fig. 1a. In addition, there are outer strengthening layers at ±45° which are each about 4.4 mm thick. Again this strip is glued to aluminum partial disks. The composite specimens in Fig. 1a and b are employed to measure the interface fracture toughness $\mathscr{G}_{ic}$ for a crack along the interface between two layers with fibers along different directions. In particular, the delamination toughness for a 0°/90° pair of fiber-reinforced carbon/epoxy material is studied.

In Section 2, some basic expressions related to interface fracture for this special pair of layers are presented. Details of the material used, the specimen configuration and testing are described in Section 3. A discussion of the residual curing stresses and their effect on the stress intensity factors is given in Section 4. The M-integral which was extended for thermal loads by Banks-Sills and Dolev (2004) is employed here to obtain stress intensity factors resulting from the residual curing stresses. Specimen calibration connected with the applied load is described in Section 5. The finite element method together with an M-integral is employed to relate stress intensity factors to the applied load, loading angle and specimen geometry. Results are presented in Section 6 for a complete set of specimens. A fracture criterion is described in Section 7 and compared to the experimental results.

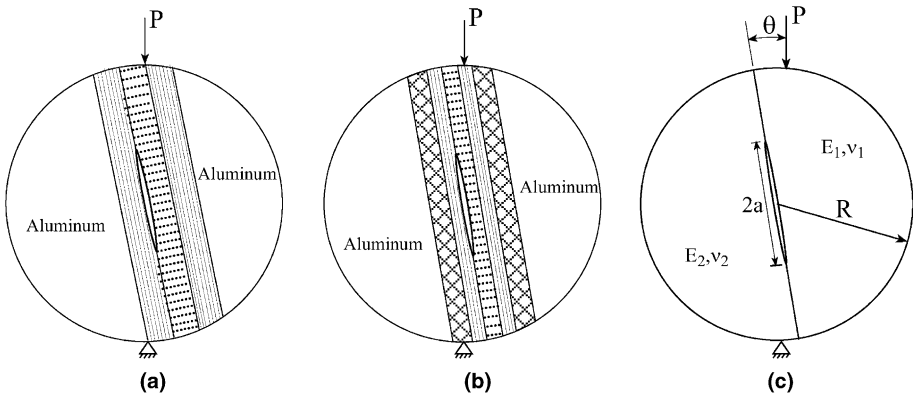

Fig. 1. Brazilian disk specimens. Composite specimens containing (a) 0°/90°/0° strip and (b) with ±45° outer stiffening layers. (c) Original bimaterial specimen.

2. Fracture mechanics of interface cracks between two anisotropic materials

Before proceeding, relevant concepts are provided for understanding interface fracture mechanics for the material pair investigated in this study. Each layer of fiber-reinforced material is transversely isotropic. The material is assumed to be homogeneous and represented by its effective mechanical properties.

For any two perfectly bonded isotropic or anisotropic materials (refer to Fig. 2), the in-plane stresses in the neighborhood of a crack tip at an interface are given by

$$\sigma_{st} = \frac{1}{\sqrt{2\pi r}}[\mathrm{Re}(Kr^{i\epsilon})\Sigma_{st}^{(1)}(\theta,\epsilon) + \mathrm{Im}(Kr^{i\epsilon})\Sigma_{st}^{(2)}(\theta,\epsilon)] \tag{1}$$

where $s, t = 1, 2$, $i = \sqrt{-1}$, the complex stress intensity factor

$$K = K_1 + iK_2 \tag{2}$$

and the superscripts (1) and (2) are related to the real and imaginary parts of $Kr^{i\epsilon}$, respectively.

In (1), following Ting (1996)

$$\epsilon = \frac{1}{2\pi}\ln\left(\frac{1+\beta}{1-\beta}\right) \tag{3}$$

where

$$\beta = \left\{-\frac{1}{2}\,\mathrm{tr}(\breve{\mathbf{S}})^2\right\}^{1/2}. \tag{4}$$

The 3×3 matrix $\breve{\mathbf{S}}$ is given by

$$\breve{\mathbf{S}} = \mathbf{D}^{-1}\mathbf{W}, \tag{5}$$

$$\mathbf{D} = \mathbf{L}_1^{-1} + \mathbf{L}_2^{-1} \tag{6}$$

and

$$\mathbf{W} = \mathbf{S}_1\mathbf{L}_1^{-1} - \mathbf{S}_2\mathbf{L}_2^{-1}. \tag{7}$$

The subscripts 1 and 2 in (6) and (7) represent, respectively, the upper and lower material. Since $\mathbf{S}_j$ and $\mathbf{L}_j$ are real and

$$-\mathbf{A}_j\mathbf{B}_j^{-1} = \mathbf{S}_j\mathbf{L}_j^{-1} + i\mathbf{L}_j^{-1}, \tag{8}$$

(no summation on j) knowledge of the left-hand side of (8) is sufficient to determine (6) and (7). The matrices $\mathbf{A}_j$ and $\mathbf{B}_j$ for transversely isotropic materials are given in Appendix A. They are 3×3 matrices related to the mechanical properties of the materials.

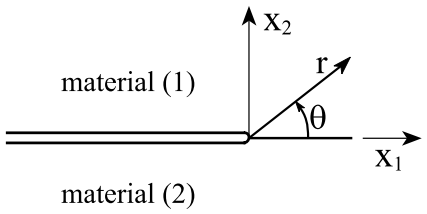

Fig. 2. Crack tip coordinates.

Referring again to the expression for the stresses in (1), the functions $\Sigma_{st}^{(1)}$ and $\Sigma_{st}^{(2)}$ are presented in Appendix 2 of Banks-Sills and Boniface (2000) for the two transversely isotropic materials considered in this study. For two isotropic materials they are given in polar coordinates by Rice et al. (1990) and in Cartesian coordinates by Deng (1993).

The complex stress intensity factor in (2) may be normalized as

$$\tilde{K} = \frac{KL^{i\epsilon}}{\sigma\sqrt{\pi L}} \tag{9}$$

where L is an arbitrary length parameter and σ is the applied stress. The non-dimensional complex stress intensity factor may be written as

$$\tilde{K} = |K|e^{i\psi}, \tag{10}$$

so that the phase angle or mode mixity

$$\psi = \arctan\left[\frac{\Im(K\,L^{i\epsilon})}{\Re(K\,L^{i\epsilon})}\right] = \arctan\left[\sqrt{\frac{D_{11}}{D_{22}}}\frac{\sigma_{12}}{\sigma_{22}}\right]\Bigg|_{\theta=0,r=L}. \tag{11}$$

In (11)

$$D_{11} = \frac{(\beta_1+\beta_2)}{E_A}\left(1 - \nu_A^2\frac{E_T}{E_A}\right) + \frac{1+2\kappa}{4G_T}, \tag{12}$$

$$D_{22} = \frac{\beta_1\beta_2(\beta_1+\beta_2)}{E_A}\left(1 - \nu_A^2\frac{E_T}{E_A}\right) + \frac{1+2\kappa}{4G_T}. \tag{13}$$

The material parameters D_{11} and D_{22} always have the same sign; they are components of the matrix $\mathbf{D}$ in (6). The mechanical properties E_A, E_T, G_A, G_T, ν_A and ν_T are the usual material properties (namely, Young's moduli, shear moduli and Poisson's ratios) in the axial and transverse directions, respectively; since the material is transversely isotropic, $G_T = E_T/2(1+\nu_T)$. The parameter κ is given in Eq. (A.19). The constants β_j, $j = 1, 2, 3$, are related to the three complex eigenvalues of the elastic constants p_j for the upper material, where $p_j = i\beta_j$ for a transversely isotropic material with this material symmetry. They are given in Eqs. (A.2) and (A.3).

For plane strain conditions, the stress components on the interface ahead of the crack tip are

$$\left(\sqrt{\frac{D_{22}}{D_{11}}}\sigma_{22} + i\sigma_{12}\right)\Bigg|_{\theta=0} = \frac{Kr^{i\epsilon}}{\sqrt{2\pi r}}. \tag{14}$$

The crack face displacements in the vicinity of the crack tip are found to be

$$\sqrt{\frac{D_{11}}{D_{22}}}\Delta u_2 + i\Delta u_1 = \frac{2D_{11}}{(1+2i\epsilon)\cosh\pi\epsilon}\sqrt{\frac{r}{2\pi}}Kr^{i\epsilon} \tag{15}$$

where $\Delta u_j = u_j^{(1)}(r,\pi) - u_j^{(2)}(r,-\pi)$.

The interface energy release rate $\mathscr{G}_i$ is related to the stress intensity factors by

$$\mathscr{G}_i = \frac{1}{H}(K_1^2 + K_2^2) \tag{16}$$

where

$$\frac{1}{H} = \frac{D_{11}}{4\cosh^2\pi\epsilon}. \tag{17}$$

Note that the subscript 'i' in (16) represents interface and $\mathscr{G}_i$ has units of force per length.

It should be noted that inherently for any interface both K_1 and K_2 must be prescribed or equivalently $\mathcal{G}_i$ and ψ. In describing an interface crack propagation criterion, one may prescribe a relation between K_1 and K_2 or what is commonly done, the critical energy release rate $\mathcal{G}_{ic}$ is given as a function of the phase angle ψ.

3. Specimen details and testing

Laminates made from graphite/epoxy (AS4/3502) prepregs are cured in an autoclave at high temperatures and pressures. As a result, residual stresses are induced within the laminate. A plate approximately 12.6 mm thick consisting of three 4.2 mm layers in the 0°/90°/0° directions was fabricated by Israel Aircraft Industries with 16 mm wide and 25.4 μm thick Teflon (FEP fluorocarbon resin) strips introduced periodically between two of the layers (see Fig. 3a). The plate was cut into long strips as illustrated in Fig. 3b. Short strips (see Fig. 3c) were taken from the long strip to be glued within the Brazilian disk specimen as seen in Fig. 1a. The short strips were rounded along the edges, rotated and inserted within the aluminum partial disks. For the specimen in Fig. 1b, a similar procedure was followed. In this case, there are three 0.54 mm thick inner layers in the 0°/90°/0° directions. Outer stiffening layers of ±45°, 4.4 mm thick, have been added to prevent plate bending.

The Brazilian disk specimens were tested to obtain the load P_c and the delamination length $2a_c$ at failure. Measurements of the specimen are carried out in the spirit of the ASTM Standard E 399-90 (1999). A crack opening displacement gauge is adapted to measure the crack sliding displacement of each specimen.

The experimental set-up is shown in Fig. 4. An Instron loading machine (model no. 1341) is employed in the testing. The test data consisting of the applied load and the crack sliding displacement is monitored by a personal computer. A video recorder, together with a stereo-microscope and a digital camera are employed to record all tests. In this way, it is possible to return to the tests and review them. A digital AV mixer is used to record the load on the video as the test proceeds.

Effective material properties of the graphite/epoxy fiber-reinforced composite are obtained by the software GMC3D based upon the generalized method of cells (Paley and Aboudi, 1992). These are presented as the computed values in Table 1. Also measurements were made by Ishai (2002) on this material, and these are presented as the measured values. The close correlation between the measured and computed values may be noted. The computed values are employed in the analyses presented in this paper.

For the composite in the specimen in Fig. 1b, additional material properties are required. These are for the ±45° layers. They have been obtained by a micromechanics model developed by Aboudi et al. (2001), and are presented in Table 2. It may be noted that the subscripts refer to the coordinate directions in Fig. 2. The Poisson ratios are defined so that $\nu_{ij} = -\epsilon_j/\epsilon_i$ where contracted notation is used for the strain.

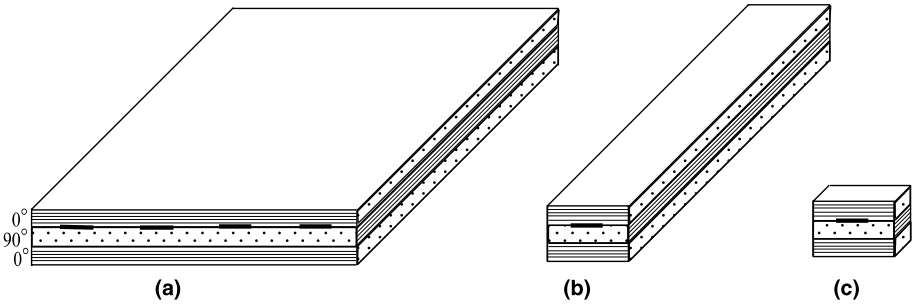

Fig. 3. (a) Sketch of plate fabricated by IAI. (b) Long strip taken from plate and (c) short strip including one crack.

Fig. 4. Experimental set-up.

Table 1
Some material properties of graphite/epoxy (AS4/3502) fiber-reinforced composite ($V_f = 0.62$)

Property	Computed	Measured
E_A (GPa)	138.0	137.0
E_T (GPa)	9.7	9.8
G_A (GPa)	4.6	5.9
ν_A	0.32	0.34
ν_T	0.46	
α_A/°C	-0.5×10^{-6}	
α_T/°C	36.6×10^{-6}	

Table 2
Material properties of the ±45° layers of graphite/epoxy (AS4/3502) fiber-reinforced composite ($V_f = 0.62$)

Property	Value
E_{11} (GPa)	12.5
E_{22} (GPa)	12.5
E_{33} (GPa)	9.7
G_{12} (GPa)	13.1
G_{13} (GPa)	3.9
G_{23} (GPa)	3.9
ν_{12}	0.35
ν_{13}	0.30
ν_{32}	0.30
α_{11}/°C	18.0×10^{-6}
α_{22}/°C	18.0×10^{-6}
α_{33}/°C	36.6×10^{-6}

4. Residual curing stresses

The following description refers to the specimen in Fig. 1a; it may be applied to the specimen in Fig. 1b, as well. The composite plate in Fig. 3a is cured according to the manufacturer instructions (177 °C and 85

psi). It is observed that a series of transverse cracks develop within the 90° layer. As an example, a set of equally spaced periodic transverse cracks are shown in Fig. 5. In the actual laminate they are not equally spaced as may be observed in Fig. 6a and b. Residual stresses, resulting from the curing process, induce mode 1 and 2 stress intensity factors at the delamination tips. These must be calculated in order to correctly determine the interface delamination toughness. In addition, the transverse cracks also affect these stress intensity factors.

The residual stresses for the laminate in Fig. 5 were determined by four methods in Banks-Sills et al. (2003). Stress intensity factors resulting from these stresses were determined using the superposition principle. A more efficient and accurate method, the thermal M-integral, was developed and presented in Banks-Sills and Dolev (2004). As an example, the structure in Fig. 5 containing a periodic array of cracks is analyzed. Comparison is made between stress intensity factors obtained by means of the superposition principle with the residual stresses computed from a finite element solution, and the thermal-elastic M-integral. In both cases, the transverse cracks in Fig. 5 are accounted for. It should be noted that it was shown in Banks-Sills et al. (2003) that transverse cracks affect the values of stress intensity factors.

A finite element mesh of the entire strip in Fig. 5 consisting of approximately 20,000 eight noded isoparametric elements and 65,000 nodal points is created. The number of elements and nodal points varies depending upon the position of the delamination relative to the transverse cracks. Mesh refinement was examined. In addition, the J-integral of ADINA (Bathe, 2000) which does not allow for mode separation was used to check the accuracy of the results obtained for each strip that was analyzed with residual stresses. It may be noted that ADINA directly calculates the J-integral for a temperature change.

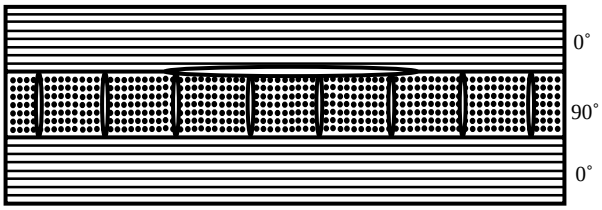

Fig. 5. Laminate with 90° layer containing transverse cracks.

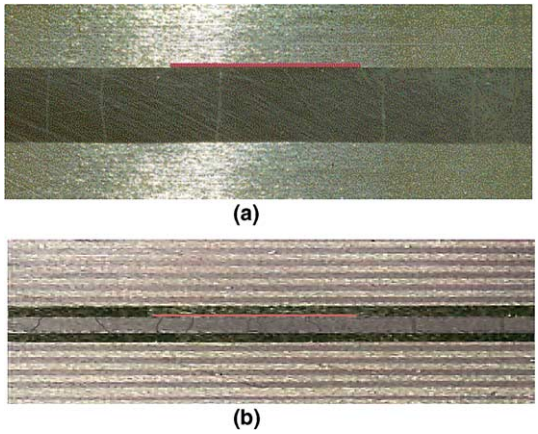

Fig. 6. Actual laminates with 90° layer containing transverse cracks. Laminates corresponding to (a) Fig. 1a and (b) Fig. 1b.

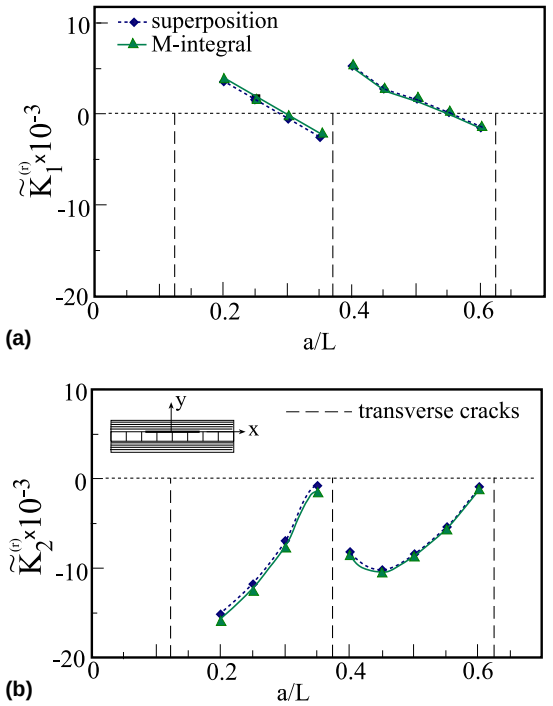

Fig. 7. Normalized stress intensity factors resulting from the residual stresses and transverse cracks for (a) mode 1 and (b) mode 2.

The stress intensity factors are normalized using Eq. (9) where $L = \ell$ in the numerator (ℓ is taken as the nominal fiber diameter of 20 μm), $L = a$ in the denominator (a is half crack length), $\sigma = E_A \Delta\alpha \Delta T$, $\Delta\alpha = \alpha_T - \alpha_A$ and $\Delta T = -150$ °C. The normalized stress intensity factors are illustrated in Fig. 7.

It may be observed in Fig. 7 that the transverse cracks act to lower the stress intensity factors. This is evident from the fact that both $\widetilde{K}_1^{(r)}$ and $\widetilde{K}_2^{(r)}$ tend to zero in the vicinity of transverse cracks. There are slight differences between the stress intensity factors computed by means of the M-integral and superposition methods. Since the transverse cracks cause complications with the superposition method, it is concluded that the M-integral leads to more exact results, and is used in the analyses presented herein.

For each specimen tested, the stress intensity factors resulting from the residual stresses and transverse cracks in the 90° layer are obtained. It may be noted that each specimen has a different transverse crack pattern. A typical mesh of the composite strip consists of approximately 23,500 eight noded isoparametric elements and 72,000 nodal points.

5. Specimen calibration

In addition, the stress intensity factors resulting from the load P applied to the Brazilian disk specimens as shown in Fig. 1a and b are required. To this end, finite element analyses to determine the stress and displacement field are carried out. The program ADINA (Bathe, 2000) is employed. The conservative M-integral developed for this material pair by Banks-Sills and Boniface (2000) is used to extract the stress intensity factors. An analysis of each specimen is required. The analyses account for delamination length and load at failure, transverse crack pattern and crack eccentricity. A typical mesh consists of approximately 27,300 eight noded isoparametric elements and 83,400 nodal points.

The total '(T)' stress intensity factors are obtained by superposition to be

$$K_1^{(\mathrm{T})} = K_1^{(\mathrm{f})} + K_1^{(\mathrm{r})}, \tag{18}$$

$$K_2^{(\mathrm{T})} = K_2^{(\mathrm{f})} + K_2^{(\mathrm{r})} \tag{19}$$

where '(f)' represents applied load and '(r)' residual stresses. Eqs. (18) and (19) are substituted into (16) and (11) to obtain, respectively, the critical interface energy release rate $\mathcal{G}_{\mathrm{ic}}$ and the mode mixity or phase angle ψ. In Section 6, results for successful tests are presented.

6. Results

The interface toughness results are reported here. The loading angle θ, as well as the load and crack length at fracture, P_c and $2a_c$ are presented in Tables 3 and 4. Table 3 is for the specimen in Fig. 1a and Table 4 is for the specimen in Fig. 1b. The stress intensity factors resulting from the loading $K_1^{(\mathrm{f})}$ and $K_2^{(\mathrm{f})}$ are calculated by means of the finite element method and the regular M-integral. These are also presented in Tables 3 and 4. The individual crack patterns for each specimen, as well as crack eccentricity are accounted for in the finite element calculation.

It may be observed in Table 3 that most of the cracks grew with the loading angle θ negative. In considering Fig. 1a, a negative angle θ is equivalent to either the crack propagating from the lower crack tip or rotation of the specimen. For all those specimens except specimen 92, the crack propagated from the bottom tip. With some specimens, it is possible to see in a video review of the test, from which tip the crack propagates. In others, the delamination deformation pattern enabled prediction of the propagating crack tip. This will be described in the sequel.

The stress intensity factors resulting from the residual stresses are calculated by means of the thermal-elastic M-integral (Banks-Sills and Dolev, 2004). These results are presented in Tables 5 and 6 for the specimens in Fig. 1a and b, respectively.

By the superposition principle in (18) and (19) the total stress intensity factors are obtained and presented in Tables 7 and 8 for the specimens in Fig. 1a and b, respectively. The interface toughness values

Table 3
Test results from specimen loading for the 0°/90° interface employing the specimen in Fig. 1a

Specimen no.	θ (deg)	P_c (N)	$2a_c$ (mm)	$K_1^{(\mathrm{f})}$ (MPa $\sqrt{m}(m)^{i\epsilon}$)	$K_2^{(\mathrm{f})}$ (MPa $\sqrt{m}(m)^{i\epsilon}$)
47	10	2740	15.24	0.501	1.141
55	5	3980	15.71	1.077	1.085
82	5	3780	15.34	0.453	0.545
96	5	4006	16.68	1.062	1.182
77	2	3830	16.10	0.658	0.145
81	0	5000	17.29	0.793	−0.0839
83	−2	4000	16.83	0.462	−0.709
98	−2	4480	15.86	0.878	−0.349
99	−2	3650	15.89	0.664	−0.453
100	−2	4280	17.57	0.913	−0.268
72	−5	3031	15.81	0.698	−0.279
79	−5	3094	15.80	−0.0377	−1.117
97	−5	3630	15.55	0.546	−0.763
59	−10	3420	15.96	0.449	−0.970
67	−10	2700	15.81	0.926	−0.488
92	−10	4560	17.25	0.703	−1.450

Table 4
Test results from specimen loading for the 0°/90° interface employing the specimen in Fig. 1b

Specimen no.	θ (deg)	P_c (N)	$2a_c$ (mm)	$K_1^{(f)}$ (MPa $\sqrt{m}(m)^{i\epsilon}$)	$K_2^{(f)}$ (MPa $\sqrt{m}(m)^{i\epsilon}$)
140	−13	4683	14.63	0.467	−1.525
142	−13	4764	15.01	0.607	−1.386
118	−10	4365	14.50	0.635	−1.170
119	−10	4050	15.84	0.581	−1.180
127	−5	3464	15.41	0.807	−0.504
129	−5	3293	15.59	0.611	−0.669
144	−2	4404	14.99	0.860	−0.449
145	−2	4433	15.76	0.822	−0.499

Table 5
The residual stress intensity factors of the 0°/90° interface for the specimen in Fig. 1a

Specimen no.	$K_1^{(r)}$ (MPa $\sqrt{m}(m)^{i\epsilon}$)	$K_2^{(r)}$ (MPa $\sqrt{m}(m)^{i\epsilon}$)
47	0.649	−0.198
55	0.365	1.094
82	0.230	0.523
96	0.241	0.910
77	−0.144	−0.318
81	−0.546	−0.817
83	−0.298	−0.654
98	−0.528	−1.327
99	−0.473	−1.085
100	−0.509	−0.756
72	−0.556	−0.586
79	0.465	0.784
97	−0.449	−1.176
59	−0.502	−1.046
67	−0.657	−0.724
92	−0.507	−1.059

Table 6
The residual stress intensity factors of the 0°/90° interface for the specimen in Fig. 1b

Specimen no.	$K_1^{(r)}$ (MPa $\sqrt{m}(m)^{i\epsilon}$)	$K_2^{(r)}$ (MPa $\sqrt{m}(m)^{i\epsilon}$)
140	−0.352	−0.153
142	−0.442	−0.255
118	−0.313	−0.0827
119	−0.429	0.115
127	−0.615	−0.338
129	−0.326	−0.0309
144	−0.324	−0.083
145	−0.398	−0.0585

$\mathcal{G}_{ic}$ and the corresponding mode mixity or phase angle ψ obtained from (16) and (11)), respectively, are exhibited. The length L in (11) is taken to be $L = 100$ μm. This value approximately centers the experimental results about $\psi = 0$. The oscillatory parameter $\epsilon = -0.03627$. Thus, although for specimen 59 both

Table 7
Test results for the 0°/90° interface (specimen type shown in Fig. 1a), $L = 100$ μm

Specimen no.	θ (deg)	$K_1^{(T)}$ (MPa $\sqrt{m}(m)^{i\epsilon}$)	$K_2^{(T)}$ (MPa $\sqrt{m}(m)^{i\epsilon}$)	$\mathcal{G}_{ic}$ (N/m)	ψ (deg)
47	10	1.150	0.923	135.3	58.5
55	5	1.442	2.179	417.6	75.6
82	5	0.683	1.068	324.2	71.9
96	5	1.303	2.092	371.4	77.2
77	2	0.513	−0.175	18.0	0.46
81	0	0.247	−0.900	53.3	−55.5
83	−2	0.164	−1.362	115.2	−64.5
98	−2	0.350	−1.675	179.2	−55.1
99	−2	0.191	−1.538	146.9	−63.8
100	−2	0.403	−1.024	74.0	−49.4
72	−5	0.143	−0.865	47.0	−61.5
79	−5	0.427	−0.332	19.9	−18.8
97	−5	0.0974	−1.939	230.5	−68.0
59	−10	−0.0230	−2.016	248.6	−71.5
67	−10	0.269	−1.212	94.3	−58.3
92	−10	0.196	−2.509	387.3	−66.4

Table 8
Test results for the 0°/90° interface (specimen type shown in Fig. 1b), $L = 100$ μm

Specimen no.	θ (deg)	$K_1^{(T)}$ (MPa $\sqrt{m}(m)^{i\epsilon}$)	$K_2^{(T)}$ (MPa $\sqrt{m}(m)^{i\epsilon}$)	$\mathcal{G}_{ic}$ (N/m)	ψ (deg)
140	−13	0.115	−1.678	173.1	−66.9
142	−13	0.165	−1.641	166.4	−65.1
118	−10	0.322	−1.253	102.3	−56.4
119	−10	0.152	−1.065	70.8	−62.7
127	−5	0.191	−0.842	45.7	−58.1
129	−5	0.285	−0.670	34.9	−48.7
144	−2	0.537	−0.532	34.9	−25.6
145	−2	0.424	−0.557	30.0	−33.6

values of the stress intensity factor are negative, the term $\epsilon \ln L$ (implicit in (11)) translates the phase angle or mode mixity from the third to the second quadrant. It may also be observed that there is not a one-to-one correlation between the loading angle θ and the phase angle ψ as there generally is for isotropic bimaterials.

This lack of correlation is related to the transverse crack pattern in the 90° layer, as well as crack eccentricity. For specimen, 79 there is one transverse crack near the crack tip which does not propagate as illustrated in Fig. 8a. For the other specimens in this group there are usually two or three transverse cracks along the delamination. A more typical crack pattern for these specimens may be observed in Fig. 8b for specimen 72. The presence and position of the transverse cracks affect the mode mixity. Considering these two specimens, although they are tested at the same loading angle, namely $\theta = -5°$, the interface toughness $\mathcal{G}_{ic}$ and phase angle ψ are greatly affected (see Table 7). Moreover, it may be noted that for the group of specimens in Table 8 (Fig. 1b), there any many more transverse cracks in the 90° layer as may be observed, for example, for specimen 127 in Fig. 8c, which is typical. From the deformed configuration, it is also possible to observe that the upper crack tip (right crack tip) is closed for specimens 79 and 72 (see Fig. 8a and b) and hence the crack propagates from the lower tip. For all specimens of the type in Fig. 8c including specimen 127, the crack propagated from the lower tip as was observed from the specimen.

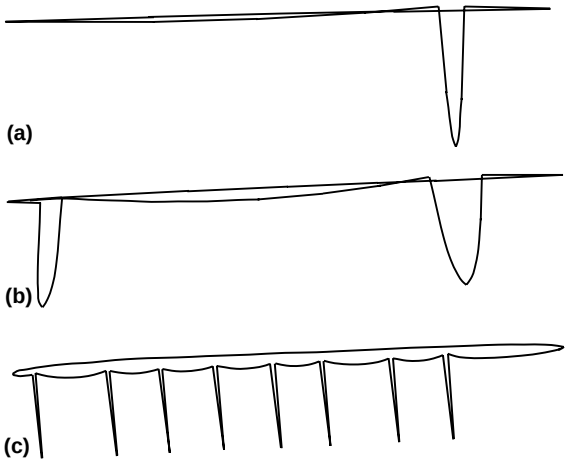

Fig. 8. Transverse crack patterns and deformation of the delamination for specimens (a) 79, (b) 72 and (c) 127.

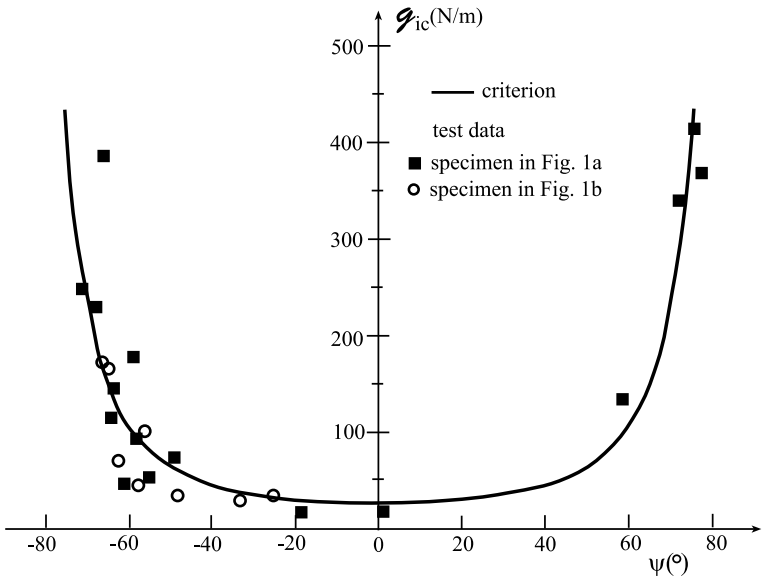

Fig. 9. Delamination toughness $\mathcal{G}_{ic}$ along a 0°/90° interface as a function of mode mixity ψ ($L = 100$ μm) for graphite/epoxy (AS4/3502). The criterion is presented in Section 7.

Results for $\mathcal{G}_{ic}$ of the specimens in Fig. 1a and b are exhibited in Fig. 9. It may be observed that the specimens in Fig. 1b fit well with those from Fig. 1a. We can conclude that the lay-up differences were accounted for in the analyses and a material property, namely, delamination toughness, has been measured.

7. Fracture criterion

An energy based fracture criterion was described by Banks-Sills and Ashkenazi (2000) for a crack on the interface between two linear elastic, isotropic, homogeneous materials. These same ideas may be applied

here. For completeness, the derivation is presented here. Eq. (16) for the interface energy release rate may be written in terms of the normalized stress intensity factor as

$$\mathscr{G}_{\mathrm{i}} = \frac{1}{H}\{[\Re(KL^{\mathrm{i}\epsilon})]^2 + [\Im(KL^{\mathrm{i}\epsilon})]^2\}. \tag{20}$$

Factoring out the first expression in curly brackets leads to

$$\mathscr{G}_{\mathrm{ic}} = \mathscr{G}_1(1 + \tan^2\psi) \tag{21}$$

where the phase angle ψ is given in Eq. (11) and

$$\mathscr{G}_1 = \frac{1}{H}[\Re(KL^{\mathrm{i}\epsilon})]^2. \tag{22}$$

There are several methods for determining the value of $\mathscr{G}_1$. Here it was found by taking the average of all values of $\Re(KL^{\mathrm{i}\epsilon})$ from the specimens in Fig. 1a and substituting it into (22). The value of H is obtained from (17). It is found here to be 16.35 GPa; so that, $\mathscr{G}_1 = 26.5$ N/m. It may be noted that in Standard D 5528-94a (2001) a value for $\mathscr{G}_{\mathrm{Ic}}$ of AS4/3501-6 is given as 85 ± 15 N/m. In Aliyu and Daniel (1985) and Gillespie et al. (1987) this value was seen to be about 200 N/m. For AS4/3502, $\mathscr{G}_{\mathrm{Ic}}$ was found to be 161 N/m (see Whitney et al. (1982)). These values are for a uni-directional composite with all fibers in the 0° direction.

It may be observed that the solid curve in Fig. 9 representing the failure curve in Eq. (21) fits relatively well with all of the test values including those obtained with the specimens illustrated in Fig. 1b. It should be emphasized that these test results were not employed to obtain $\mathscr{G}_1$. Thus, this curve may be employed to predict delamination failure along a 0°/90° interface in any structure constructed from the material studied here. For a given structure, stress intensity factors $K_1^{(\mathrm{T})}$ and $K_2^{(\mathrm{T})}$ at a typical delamination must be determined. With $L = 100$ μm, these values are substituted into (11) and (16) to obtain ψ and $\mathscr{G}_{\mathrm{i}}$, respectively. The critical toughness value $\mathscr{G}_{\mathrm{ic}}$ for this value of ψ is obtained from the graph in Fig. 9. If the calculated $\mathscr{G}_{\mathrm{i}}$ value is less than $\mathscr{G}_{\mathrm{ic}}$, failure is not predicted.

8. Summary and conclusions

Interface toughness values have been obtained for two series of specimens with different lay-up sequences. One lay-up consisted of three layers of approximately 4.2 mm each, 0°/90°/0°; the second lay-up consisted of five layers: ±45°/0°/90°/0°/±45°. For the second lay-up, the outer layers were about 4.4 mm thick and each of the inner three layers was about 0.54 mm thick. In both cases a delamination was placed along the 0°/90° interface by means of a Teflon strip 25.4 μm thick. Tests were carried out on these specimens; values for the load and crack length at fracture were measured. The tests were performed in the spirit of ASTM fracture toughness testing. In these tests, three factors contributed to the toughness: the loading, the residual curing stresses and transverse cracks in the 90° layer. The contribution of the loading was obtained by means of a finite element analysis and an M-integral. Since it was seen in an earlier investigation (Banks-Sills et al., 2003) that the transverse cracks in the 90° layer affect the stress intensity factor computations significantly, they were accounted for here. The contribution of the residual stresses was obtained by means of the finite element method and a thermal-elastic M-integral. The two components of the stress intensity factor are superposed to obtain the delamination toughness $\mathscr{G}_{\mathrm{ic}}$ as a function of the phase angle ψ. An energy based fracture criterion was presented which fits the experimental data well. It was observed that the delamination toughness values $\mathscr{G}_{\mathrm{ic}}$ obtained from the different specimen types were in good agreement.

Acknowledgment

We would like to thank Ms. Navah Sela of Israel Aircraft Industries for providing us with the composite plate. Her cooperation and our interesting conversations are gratefully acknowledged. In addition, we would also like to thank Dr. Victor Fourman for constructing all of the specimens and assisting us with the experiments.

Appendix A. Matrices $\mathbf{A}_j$, $\mathbf{B}_j$ and $\mathbf{B}_j^{-1}$ for upper and lower materials

For completeness, the matrices $\mathbf{A}_j$, $\mathbf{B}_j$ and $\mathbf{B}_j^{-1}$ which appear in (8) and are employed to calculate the oscillating part of the singularity ϵ in (3) are presented for the specific transversely isotropic materials studied here. They are also given in Appendix A of Banks-Sills and Boniface (2000). They are related to the material properties. The subscript j represents the upper and lower materials, 1 and 2, respectively.

The x_1-direction is the axial direction of the upper material. The matrix $\mathbf{A}_1$ is given by

$$\mathbf{A}_1 = -\begin{bmatrix} k_1^{(1)}Q_1 & k_2^{(1)}Q_2 & 0 \\ \mathrm{i}k_1^{(1)}Q_3/\beta_1 & \mathrm{i}k_2^{(1)}Q_4/\beta_2 & 0 \\ 0 & 0 & -\mathrm{i}k_3^{(1)}/\beta_3 G_\mathrm{T} \end{bmatrix} \tag{A.1}$$

where $k_j^{(1)}$, $j = 1, 2, 3$, are normalization factors for the upper material which are not necessary in the calculation of (8). The constants β_j, $j = 1, 2, 3$ are related to the three complex eigenvalues of the elastic constants p_j (see Ting, 1996, pp. 121–128), where $p_j = \mathrm{i}\beta_j$ for a transversely isotropic material with this material symmetry. They are given by

$$\beta_{1,2} = \left[\frac{(2s'_{12} + s'_{66}) \mp \sqrt{(2s'_{12} + s'_{66})^2 - 4s'_{11}s'_{22}}}{2s'_{11}}\right]^{1/2}, \tag{A.2}$$

$$\beta_3 = \sqrt{s'_{44}/s'_{55}} \tag{A.3}$$

where s'_{ij} are elements of the reduced compliance matrix, which for the present material are found to be

$$s'_{11} = \left(1 - \nu_\mathrm{A}^2 \frac{E_\mathrm{T}}{E_\mathrm{A}}\right)\frac{1}{E_\mathrm{A}}, \tag{A.4}$$

$$s'_{12} = -(1 + \nu_\mathrm{T})\frac{\nu_\mathrm{A}}{E_\mathrm{A}}, \tag{A.5}$$

$$s'_{22} = \frac{(1 - \nu_\mathrm{T}^2)}{E_\mathrm{T}}, \tag{A.6}$$

$$s'_{44} = \frac{2(1 + \nu_\mathrm{T})}{E_\mathrm{T}}, \tag{A.7}$$

$$s'_{55} = s'_{66} = \frac{1}{G_\mathrm{A}}. \tag{A.8}$$

The constants Q_i are related to the material properties as

$$Q_1 = \frac{1}{E_A}[\beta_1^2(1 - v_A^2 E_T/E_A) + v_A(1 + v_T)], \tag{A.9}$$

$$Q_2 = \frac{1}{E_A}[\beta_2^2(1 - v_A^2 E_T/E_A) + v_A(1 + v_T)], \tag{A.10}$$

$$Q_3 = (1 + v_T)[\beta_1^2 v_A/E_A + (1 - v_T)/E_T], \tag{A.11}$$

$$Q_4 = (1 + v_T)[\beta_2^2 v_A/E_A + (1 - v_T)/E_T]. \tag{A.12}$$

The material parameters E_A, E_T, G_A, G_T, v_A and v_T are the usual material properties in the axial and transverse directions (namely, Young's moduli, shear moduli and Poisson's ratios); since the material is transversely isotropic, $G_T = E_T/2(1 + v_T)$.

The matrix $\mathbf{B}_1$ is given by

$$\mathbf{B}_1 = \begin{bmatrix} -ik_1^{(1)}\beta_1 & -ik_2^{(1)}\beta_2 & 0 \\ k_1^{(1)} & k_2^{(1)} & 0 \\ 0 & 0 & -k_3^{(1)} \end{bmatrix}. \tag{A.13}$$

Its inverse is given by

$$\mathbf{B}_1^{-1} = \frac{1}{\beta_2 - \beta_1}\begin{bmatrix} -i/k_1^{(1)} & \beta_2/k_1^{(1)} & 0 \\ i/k_2^{(1)} & -\beta_1/k_2^{(1)} & 0 \\ 0 & 0 & -(\beta_2 - \beta_1)/k_3^{(1)} \end{bmatrix}. \tag{A.14}$$

In the lower material, the axial direction coincides with the x_3-direction. The mechanical properties E_A, E_T, G_A, G_T, v_A and v_T are taken to be the same as for the upper material; but they are in different coordinate directions. It turns out that this material is mathematically degenerate. It has three identical complex eigenvalues $p_j = i$ where the subscript $j = 1, 2, 3$. To determine the stress and displacement fields, matrices alternative to $\mathbf{A}_2$ and $\mathbf{B}_2$ are required; these are $\mathbf{A}_2'$ and $\mathbf{B}_2'$. Since

$$\mathbf{A}\mathbf{B}^{-1} = \mathbf{A}'\mathbf{B}'^{-1}, \tag{A.15}$$

it is possible to calculate ϵ with the aid of (8). On the other hand, one may determine $\mathbf{A}_2\mathbf{B}_2^{-1}$ without calculating the individual matrices (see Ting, 1996, p. 173).

For brevity, only the primed matrices are presented. To obtain them, an orthogonalization procedure is employed; for details see Ting (1996, pp. 489–492) and Ting and Hwu (1988). They are found to be

$$\mathbf{A}_2' = \begin{bmatrix} k_1^{(2)} & -ik_1^{(2)}\kappa & 0 \\ ik_1^{(2)} & -k_1^{(2)}\kappa & 0 \\ 0 & 0 & k_3^{(2)} \end{bmatrix}, \tag{A.16}$$

$$\mathbf{B}_2' = \begin{bmatrix} 2iG_T k_1^{(2)} & G_T k_1^{(2)} & 0 \\ -2G_T k_1^{(2)} & -iG_T k_1^{(2)} & 0 \\ 0 & 0 & iG_A k_3^{(2)} \end{bmatrix} \tag{A.17}$$

and

$$\mathbf{B}_2'^{-1} = \begin{bmatrix} -\mathrm{i}/(4G_\mathrm{T}k_1^{(2)}) & -1/(4G_\mathrm{T}k_1^{(2)}) & 0 \\ 1/(2G_\mathrm{T}k_1^{(2)}) & \mathrm{i}/(2G_\mathrm{T}k_1^{(2)}) & 0 \\ 0 & 0 & -\mathrm{i}/(G_\mathrm{A}k_3^{(2)}) \end{bmatrix} \tag{A.18}$$

where

$$\kappa = \frac{3 - \nu_\mathrm{T} - 4\nu_\mathrm{A}^2 E_\mathrm{T}/E_\mathrm{A}}{2(1+\nu_\mathrm{T})}. \tag{A.19}$$

The normalization factors $k_1^{(2)}$ and $k_3^{(2)}$ are again unnecessary for determining both β and the stress and displacement fields. Nonetheless, for this special case of a mathematically degenerate material, they are seen to be

$$k_1^{(2)} = \frac{1}{4\sqrt{E_\mathrm{T}(1 - \nu_\mathrm{A}^2 E_\mathrm{T}/E_\mathrm{A})}}, \tag{A.20}$$

$$k_3^{(2)} = \frac{(1-\mathrm{i})}{2\sqrt{G_\mathrm{A}}}. \tag{A.21}$$

References

Aboudi, J., Pindera, M.-J., Arnold, S.M., 2001. Linear thermoelastic higher-order theory for periodic multiphase materials. Journal of Applied Mechanics 68, 697–707.

Aliyu, A.A., Daniel, I.M., 1985. Effects of strain rate on delamination fracture toughness of graphite/epoxy. In: Johnson, W.S. (Ed.), Delamination and Debonding of Materials, ASTM-STP 876. American Society for Testing and Materials, Philadelphia, pp. 336–348.

ASTM Standard, 1999. Standard test method for plane-strain fracture toughness of metallic materials, E 399-90 (reapproved 1997). In: Annual Book of ASTM Standards 03.01. American Society for Testing and Materials, Philadelphia.

ASTM Standard, 2001. Standard test method for mode I interlaminar fracture of unidirectional fiber-reinforced polymer matrix composites, D 5528-94a. In: Annual Book of ASTM Standards 15.03. American Society for Testing and Materials, Philadelphia.

ASTM Standard, 2002. Standard test method for mixed mode I-mode II interlaminar fracture of unidirectional fiber-reinforced polymer matrix composites, D 6671-01. In: Annual Book of ASTM Standards 15.03. American Society for Testing and Materials, Philadelphia.

Banks-Sills, L., Ashkenazi, D., 2000. A note on fracture criteria for interface fracture. International Journal of Fracture 103, 177–188.

Banks-Sills, L., Boniface, V., 2000. Fracture mechanics for an interface crack between a special pair of transversely isotropic materials. In: Chuang, T.-J., Rudnicki, J.W. (Eds.), Multiscale Deformation and Fracture in Materials and Structures—The James R. Rice 60th Anniversary Volume. Kluwer Academic Publishers, The Netherlands, pp. 183–204.

Banks-Sills, L., Boniface, V., Eliasi, R., 2003. Effect of residual stresses on delamination cracks in fiber reinforced composites. Interface Science 11, 339–348.

Banks-Sills, L., Dolev, O., 2004. The conservative *M*-integral for thermal-elastic problems. International Journal of Fracture 125, 149–170.

Bansal, A., Kumosa, M., 1995. Application of the biaxial Iosipescu method to mixed-mode fracture of unidirectional composites. International Journal of Fracture 71, 131–150.

Bathe, K.J., 2000. ADINA—Automatic dynamic incremental nonlinear analysis system, Version 7.5. Adina Engineering, Inc., USA.

Buchholz, F.-G., Rikards, R., Wang, H., 1997. Computational analysis of interlaminar fracture of laminated composites. International Journal of Fracture 86, 37–57.

Chai, H., 1984. The characterization of mode I delamination failure in non-woven, multidirectional laminates. Composites 15, 277–290.

Choi, N.S., Kinloch, A.J., Williams, J.G., 1999. Delamination fracture of multidirectional carbon-fiber/epoxy composites under mode I, mode II and mixed-mode I/II loading. Journal of Composite Materials 33, 73–100.

Davies, P., Moulin, C., Kausch, H.H., Fischer, M., 1990. Measurement of G_{Ic} and G_{IIc} in Carbon/Epoxy Composites. Composites Science and Technology 39, 193–205.

Deng, X., 1993. General crack-tip fields for stationary and steadily growing interface cracks in anisotropic bimaterials. Journal of Applied Mechanics 60, 183–189.

Gillespie Jr., J.W., Carlsson, L.A., Smiley, A.J., 1987. Rate-dependent mode I interlaminar crack growth mechanisms in graphite/epoxy and graphite/peek. Composites Science and Technology 28, 1–15.

Hashemi, S., Kinloch, A.J., Williams, J.G., 1990. The analysis of interlaminar fracture in uniaxial fibre-polymer composites. Proceedings of the Royal Society, London A 427, 173–199.

Hwu, C., Kao, C.J., Chang, L.E., 1995. Delamination fracture criteria for composite laminates. Journal of Composite Materials 29, 1962–1987.

Ishai, O., 2002. Personal communication.

Jurf, R.A., Pipes, R.B., 1982. Interlaminar fracture of composite materials. Journal of Composite Materials 16, 386–394.

Kinloch, A.J., Wang, Y., Williams, J.G., Yayla, P., 1993. The mixed-mode delamination of fibre composite materials. Composites Science and Technology 47, 225–237.

Laksimi, A., Benzeggagh, M.L., Jing, G., Hecini, M., Roelandt, J.M., 1991. Mode I interlaminar fracture of symmetrical cross-ply composites. Composites Science and Technology 41, 147–164.

Liu, C., Huang, Y., Lovato, M.L., Stout, M.G., 1997. Measurement of the fracture toughness of a fiber-reinforced composite using the Brazilian disk geometry. International Journal of Fracture 87, 241–263.

Paley, M., Aboudi, J., 1992. Micromechanical analysis of composites by the generalized cells model. Mechanics of Materials 14, 127–139.

Polaha, J.J., Davidson, B.D., Hudson, R.C., Pieracci, A., 1996. Effects of mode ratio, ply orientation and precracking on the delamination toughness of a laminated composite. Journal of Reinforced Plastics and Composites 15, 141–173.

Reeder, J.R., Crews, J.H., 1990. Mixed-mode bending method for delamination testing. American Institute of Aeronautics and Astronautics, Journal 28, 1270–1276.

Rice, J.R., Suo, Z., Wang, J.-S., 1990. Mechanics and thermodynamics of brittle interface failure in bimaterial systems. In: Rühle, M., Evans, A.G., Ashby, M.F., Hirth, J.P. (Eds.), Metal–Ceramic Interfaces. Pergamon Press, Oxford, pp. 269–294.

Rikards, R., Buchholz, F.-G., Wang, H., Bledzki, A.K., Korjakin, A., Richard, H.-A., 1998. Investigation of mixed mode I/II interlaminar fracture toughness of laminated composites by using a CTS type specimen. Engineering Fracture Mechanics 61, 325–342.

Sun, C.T., Zheng, S., 1996. Delamination characteristics of double-cantilever beam and end-notched flexure composite specimens. Composite Science and Technology 56, 451–459.

Ting, T.C.T., 1996. Anisotropic Elasticity—Theory and Applications. Oxford University Press, Oxford.

Ting, T.C.T., Hwu, C., 1988. Sextic formalism in anisotropic elasticity for almost non-semisimple matrix **N**. International Journal of Solids and Structures 24, 65–76.

Whitney, J.M., Browning, C.E., Hoogsteden, W., 1982. A double cantilever beam test for characterizing mode I delamination of composite materials. Journal of Reinforced Plastics and Composites 1, 297–313.

Wilkins, D.J., Eisenmann, J.R., Camin, R.A., Margolis, W.S., Benson, R.A., 1982. Characterizing delamination growth in graphite–epoxy. In: Reifsnider, K.L. (Ed.), Damage in Composite Materials, ASTM-STP 755. American Society for Testing and Materials, Philadelphia, pp. 168–183.

Yoon, S.H., Hong, C.S., 1990. Interlaminar fracture toughness of graphite/epoxy composite under mixed-mode deformations. Experimental Mechanics 30, 234–239.

Zhao, S., Gädke, M., Prinz, R., 1995. Mixed-mode delamination behavior of carbon/epoxy composites. Journal of Reinforced Plastics and Composites 14, 804–826.